Chalcogenide Letters Vol. 16, No. 9, September 2019, p. 443 - 448

SYNTHESIS AND OPTICAL PROPERTIES OF $Cu_2(Co_{1-x}Mn_x)SnS_4$ NANOCRYSTALS WITH TUNABLE BAND GAP

H. GUAN*, Y. FANG, X. MA
School of Materials Science and Engineering, Yancheng Institute of Technology, 9 Yinbing Street, Yancheng 224051, PR China

$Cu_2(Co_{1-x}Mn_x)SnS_4$(CCMTS) nanocrystals were successfully synthesized via solvothermal method. The analytical results from XRD, Raman and SEM indicate that stannite $Cu_2(Co_{1-x}Mn_x)SnS_4$ phases were obtained. Furthermore, UV-Vis spectroscopy indicate that the band gap of the $Cu_2(Co_{1-x}Mn_x)SnS_4$ could be accordingly tuned almost linearly between 1.45eV and 1.53eV by adjusting *x* values.

(Received June 3, 2019; Accepted September 10, 2019)

Keywords: Solar cell materials, $Cu_2(Co_{1-x}Mn_x)SnS_4$ nanocrystals, Solvothermal method, Optical properties

1. Introduction

In decades, quaternary chalcogenide semiconductors Cu_2MeSnS_4 (Me=Zn, Fe, Mn, Co, Ni) attract wide interest because of their advantageous characteristics for photovoltaic and optoelectronic applications, such as suitable direct band gaps (1.0-1.5eV), large absorption coefficients ($\alpha>10^4cm^{-1}$) [1-5]. At present, Chen revealed that the band gap of $Cu_2ZnSn(S, Se)_4$ is tuned from 1.0eV to 1.5eV by partly substituting S with Se [6]. Meanwhile, many experiments have identified that the device efficiency was improved by partly substituting S with Se, the power conversion efficiency of $Cu_2ZnSn(S,Se)_4$ has been improved to 12.6% [7]. Furthermore, other researchers also investigated that Ge and Si substitution of Sn can tailor the band gap and improve device efficiency [8-9]. Unfortunately, Ge and Se are not desirable because of cost and rare. Therefore, some researchers find that the simple method can be made to tailor the band gap and optoelectrical properties by substituting Zn with Fe, Mn and Co, which are similar to the method of substituting S with Se and Sn with Ge and Si[10-12]. We believe that the band gap of Cu_2CoSnS_4 can be tuned by substituting Co with Mn.

Various methods have been employed to synthesize Cu_2CoSnS_4 and Cu_2MnSnS_4 semiconductors, such as thermal decomposition, hot-injection, spray, sol-gel, solvothermal synthesis, electrospinning and so on[13-18]. Among them, a solvothermal synthesis method attracts a great deal of attention owing to their simpleness, low-price and no need of sophisticated instrumention. As far as we know, no reports have been found to synthesis $Cu_2(Co_{1-x}Mn_x)SnS_4$ nanocrystals by solvothermal method.

In this paper, $Cu_2(Co_{1-x}Mn_x)SnS_4$ nanocrystals were synthesized by the solvothermal method. The composition dependence of the structure and optical properties were studied.

*Corresponding author: guanhao1980@sina.com

2. Experimental details

$Cu(NO_3)_2 \cdot 3H_2O$ (Analytical Reagent, Nanshi-Reagent), $Co(CH_3COO)_2 \cdot 6H_2O$(Analytical Reagent), $Mn(CH_3COO)_2 \cdot 2H_2O$ (Analytical Reagent, Nanshi-Reagent), $SnCl_2 \cdot 2H_2O$ (Analytical Reagent, Nanshi-Reagent) and H_2NCSNH_2 (Analytical Reagent, Nanshi-Reagent) were used as raw materials. In a typical synthesis process, $Cu(NO_3)_2 \cdot 3H_2O$, $Co(CH_3COO)_2 \cdot 6H_2O$, $Mn(CH_3COO)_2 \cdot 2H_2O$, $SnCl_2 \cdot 2H_2O$, H_2NCSNH_2 in the proportion of 2:1-*x*:*x*:1:4(*x*=0, 0.2, 0.4, 0.6, 0.8, 1) were added in 40ml ethylene glycol under sustain stirring as the precursor solution. Then the precursor solution was placed in a 50ml Teflon liner. The autocaves were sealed and maintained at 200℃ for 12h. Thereafter, the autocaves were cooled down to room temperature. At last, the products were washed several times with deionized water and dried in vacuum at 80℃ for 3h before characterization.

The structure studies were carried out using a PANalytical X'Pert PRO diffractometer with Cu *Kα* radiation (λ=0.15406nm) and JY-T64000 Raman spectrometers. The microstructure was characterized by LEO-1530VP scanning electron microscope. The optical characteristics were measured using Varian Cary 5000 spectrophotometer to calculate band gap energy.

3. Results and discussion

The XRD results of $Cu_2(Co_{1-x}Mn_x)SnS_4$ nanocrystals are shown in Fig.1. From the XRD patterns, it is clear that the stannite structure of CCTS(*x*=0) was obtained while the same stannite structure of CMTS(*x*=1), which correspond to JCPDS 26-0513(CCTS) and JCPDS 51-0757 (CMTS), respectively. No impurity phase peaks are observed from all samples, indicating the high purity phase of $Cu_2(Co_{1-x}Mn_x)SnS_4$ (*x*=0, 0.2, 0.4, 0.6, 0.8, 1) nanocrystals. Meanwhile, it can be observed that the major peaks of $Cu_2(Co_{1-x}Mn_x)SnS_4$ nanocrystals shift toward the smaller angle with Mn gradually substituting for Co, which results from the lattice extension due to the smaller-radius of Co cations (r_{Co2+}=0.074nm) being substituted by the larger-radius of Mn cations (r_{Mn2+}=0.080nm). In addition, the broad full-width at half-maxima(FWHM) brought by the nanocrystals are also observed. The peak broadening effect give rise to a difficulty in identifying their phases from each other owing to their similar structure of Cu_2SnS_3, CMTS and CCTS. Then the structure of $Cu_2(Co_{1-x}Mn_x)SnS_4$ nanocrystals are further characterized by Raman spectroscopy. As can be seen in Fig. 2, there is only one strong significant peak between 325cm^{-1} and 335cm^{-1} with expected broadness for all samples. No other prominent peaks are observed, implying the absence of obvious impurity phase Cu_2SnS_3(295, 318 and 335cm^{-1}) in all samples[19-20]. It is also found in Fig. 2 that the Raman peaks systematically shift toward lower frequency as the Mn content increases. Additionally, the strong peaks at 335cm^{-1} for CCTS and 325cm^{-1} for CMTS are denoted as A_1 modes, in which all variations in frequencies of these peaks are only due to changes of bond-stretching force constants. According to the above XRD analysis, the lattice parameter increases with increasing Mn content, indicating that the bond lengths expanded. Therefore, the bond-stretching force constants of CCMTS will become weaker when Mn substitutes gradually for Co cations. Thus the A_1 mode of CCMTS shifts toward the lower frequency direction with the increase of Mn content.

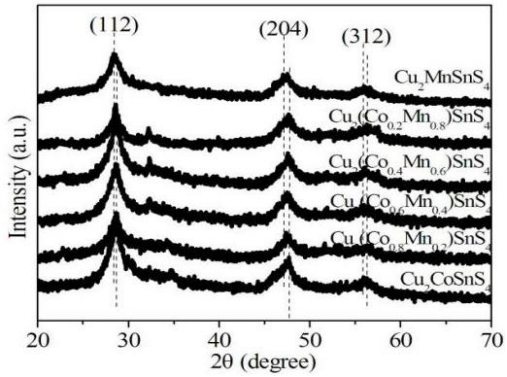

Fig. 1. XRD patterns of $Cu_2(Co_{1-x}Mn_x)SnS_4$ (x=0, 0.2, 0.4, 0.6, 0.8, 1) nanocrystals.

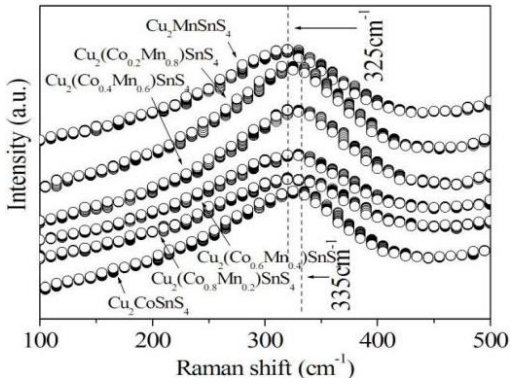

Fig. 2. Raman spectra of $Cu_2(Co_{1-x}Mn_x)SnS_4$ (x=0, 0.2, 0.4, 0.6, 0.8, 1) nanocrystals.

Fig. 3 shows the SEM images of $Cu_2(Co_{1-x}Mn_x)SnS_4$ nanocrystals. It can be seen that all samples are composed of flower-like particles. The thickness of the petals is about 50nm. $Cu_2(Co_{1-x}Mn_x)SnS_4$ can be considered as the Cu_2CoSnS_4-Cu_2MnSnS_4 pseudobinary alloyed by Cu_2CoSnS_4 and Cu_2MnSnS_4, which typically crystallize stannite type. Thus the morphologies of all samples are not change due to the same formation mechanism, which can be explained as follows: Firstly, CCMTS nanoparticles form through homogeneous nucleation and growth process. Secondly, CCMTS nanosheets are formed through oriented aggregation. At last, flower-like particles can be obtained through the self-assembly process of CCMTS nanosheets.

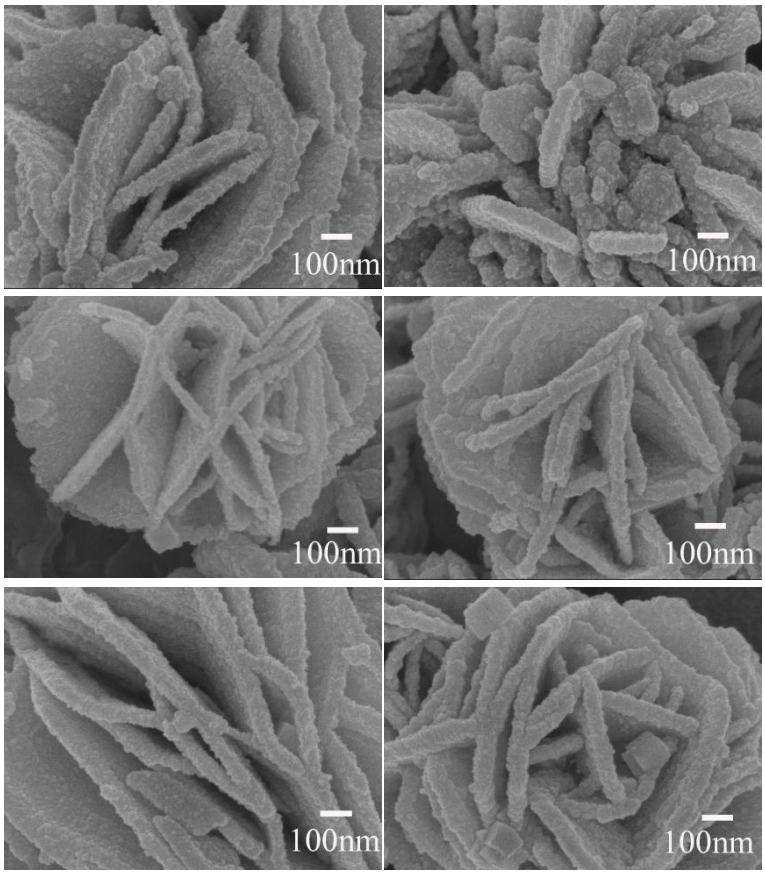

Fig. 3. SEM images of $Cu_2(Co_{1-x}Mn_x)SnS_4$ (x=0, 0.2, 0.4, 0.6, 0.8, 1) nanocrystals.

Optical properties of nanocrytals are of great importance for their potential applications in the optoelectronic field. The results of optical band gaps as a function of different *x* values are shown in Fig.4. The optical band gaps(E_g) of CCTS and CMTS nanocrystals are obtained by extrapolating the linear absorption edge part of curve to the intersection with energy axis as shown in the insert. The estimated E_g values of $Cu_2(Co_{1-x}Mn_x)SnS_4$ nanocrystals are 1.45eV, 1.47eV, 1.48eV, 1.5eV, 1.52eV and 1.53eV at x=0, 0.2, 0.4, 0.6, 0.8 and 1, respectively. Furthermore, quasi-linear relationship between the band gaps and *x* value obeys Vegard's law. Therefore, the functional dependence of the band gaps versus the Mn content provides an opportunity for the effective band engineering by varying composition in the CCMTS nanocrystals.

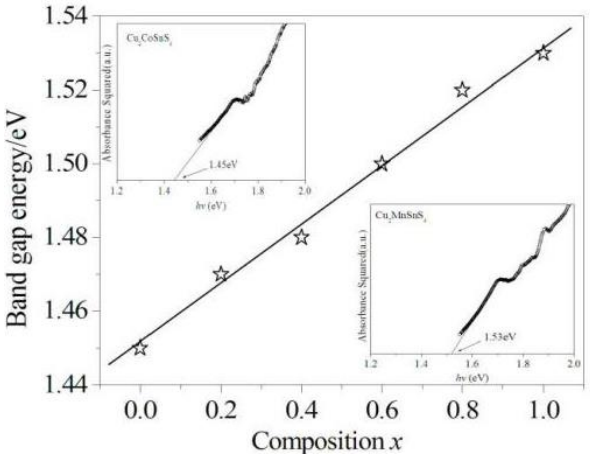

Fig. 4. The band gap as a function of x values.
Inset: Plot of absorbance squared versus hv of CMTS and CCTS nanocrystals.

4. Conclusions

In this paper, $Cu_2(Co_{1-x}Mn_x)SnS_4$ nanocrystals were synthesized by a solvothermal method. The structural, morphological and optical properties of CCMTS nanocrystals depended on Mn content were successfully illuminated. XRD and Raman analysis reveal that pure CCMTS phases were obtained. By adjusting *x* values, the band gap of the $Cu_2(Co_{1-x}Mn_x)SnS_4$ can be tuned from 1.45eV to 1.53eV. It is believed that $Cu_2(Co_{1-x}Mn_x)SnS_4$ nancrystals with tunable band gap were obtained, and it is an application opportunity for the effective band engineering.

References

[1] T. K. Todorov, J. Tang, S. Bag, O. Gunawan, T. Gokmen, Y. Zhu, D. B. Mitzi, Adv. Energy Mater. **3**, 34 (2013).
[2] X. Y. Zhang, N. Z. Bao, K. Ramasamy, Y. H. A. Wang, Y. F. Wang, B. P. Lin, A. Gupta, Chem. Commun. **48**, 4956 (2012).
[3] X. Liang, P. Guo, G. Wang, R. Deng, D. Pan, X. Wei, RSC Adv. **2**, 5044 (2012).
[4] J. Zhong, Q. Wang , W. Cai, Mater. Lett. **150**, 69 (2015).
[5] A. Kamble, K. Mokurala, A. Gupta, S. Mallick, P. Bhargava, Mater. Lett. **137**, 440 (2014).
[6] S. Chen, A. Walsh, J. H. Yang, X. G. Gong, L. Sun, P. X. Yang, J. H. Chu S. H. Wei, Phys. Rev. B: Condens. Matter Mater. Phys. **83**, 125201 (2011).
[7] W. Wang, M. T. Winkler, O. Gunawan, T. Gokmen, T. K. Todorov, Y. Zhu, D. B. Mitzi, Adv. Energy Mater. **4**, 1 (2014).
[8] G. M. Ford, Q. Guo, R. Agrawal, H. W. Hillhouse, Chem. Mater. **23**, 2626 (2011).
[9] M. Hamdi, B. Louati, A. Lafond, C. Guillot-Deudon , B. Chrif , K. Khirouni, M. Gargouri , S. Jobic, F. Hlel, J. Alloys Compd. **620**, 434 (2015).
[10] C. Huang, Y. Chan, F. Liu, D. Tang, J. Yang, Y. Lai, J. Li, Y. Liu, J. Mater. Chem. A **1**, 5402 (2013).
[11] L. Chen, H. Deng, J. Cui , J. Tao, W. Zhou, H. Cao, L. Sun, P. Yang, J. Chu. J. Alloys Compd.

627, 388 (2015).
[12] K. L Huang, C. H. Huang, W. T. Lin, Y. S. Fu,T. F. Guo, J. Alloys Compd. **646**, 1015 (2015).
[13] X. Wang, X. Gu, H. Guan, F. Yu, Chalcogenide Lett. **12**, 99 (2015).
[14] F. Ozel, J. Alloys Compd. **657**, 157 (2016).
[15] M. Krishnaiah, R. K. Mishra, S. G. Seo, S. H. Jin, J. T. Park, J Alloys Compd **781**, 1091 (2019).
[16] A. Sarilmaz, F. Ozel, J Alloys Compd. **780**, 518 (2019).
[17] T. Wang, Q. Zhan, W. Cheng, J Mater. Sci.: Mater. Electron. **30**, 2285 (2019).
[18] R. Ghediya Prashant, K. Chaudhuri Tapas, Mater. Res. Express **5**, 085509 (2018).
[19] P. A. Fernandes, P. M. P. Salome, A. F. da Cunha, J. Phys. D: Appl. Phys. **43**, 215403 (2010).
[20] A. J. Cheng, M. Manno, A. Khare, C. Leighton, S. A. Campbell, E. S. Aydil, J. Vac. Sci. Technol. **29**, 051203 (2011).